Обзор ArXiv: astro-ph, 26-30 июня 2017 года

От Сильченко О.К.

Astro-ph: 1706.08533

An extended cold gas absorber in a central cluster galaxy

Russell J. Smith* and Alastair C. Edge
Centre for Extragalactic Astronomy, University of Durham, Durham DH1 3LE, United Kingdom

MNRAS Letters, submitted 2017 June 14; accepted 2017 June 23

ABSTRACT

We present the serendipitous discovery of an extended cold gas structure projected close to the brightest cluster galaxy (BCG) of the $z = 0.045$ cluster Abell 3716, from archival integral field spectroscopy. The gas is revealed through narrow Na D line absorption, seen against the stellar light of the BCG, which can be traced for ~25 kpc, with a width of 2–4 kpc. The gas is offset to higher velocity than the BCG (by ~100 km s^{-1}), showing that it is infalling rather than outflowing; the intrinsic linewidth is ~80 km s^{-1} (FWHM). Very weak Hα line emission is detected from the structure, and a weak dust absorption feature is suggested from optical imaging, but no stellar counterpart has been identified. We discuss some possible interpretations for the absorber: as a projected low-surface-brightness galaxy, as a stream of gas that was stripped from an infalling cluster galaxy, or as a "retired" cool-core nebula filament.

MUSE: Холодная газовая структура видна в линии поглощения NaID

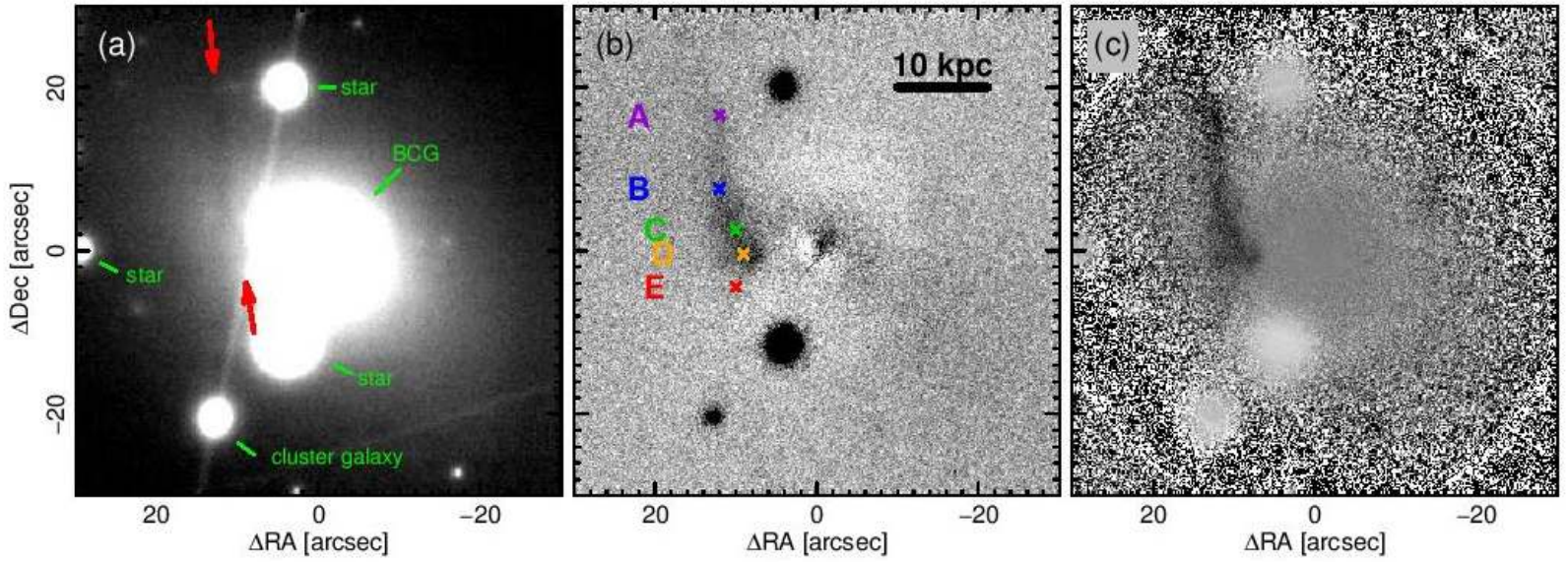

Figure 1. Image extracts from the MUSE datacube for Abell 3716. All images are presented as positives, i.e. absorption appears as darker grey. Panel (a) shows a narrow-band collapsed image at the wavelengths of the Na D absorption (6166–6179 Å); the BCG (ESO187-G026) is the bright galaxy at the field centre. The cold gas structure is visible as a faint dark streak, indicated by the red arrows, East and North of the BCG. Panel (b) shows the same spectral slice after subtracting a local continuum, and a model datacube for the BCG, to highlight the cold gas absorption more clearly. In Panel (c), the BCG model is instead *divided* into the data to form a "pseudo-equivalent-width image". Labels A–E in Panel (b) show locations also indicated in Figures 2–3.

Эта линия поглощения смещена относительно BCG в красную сторону

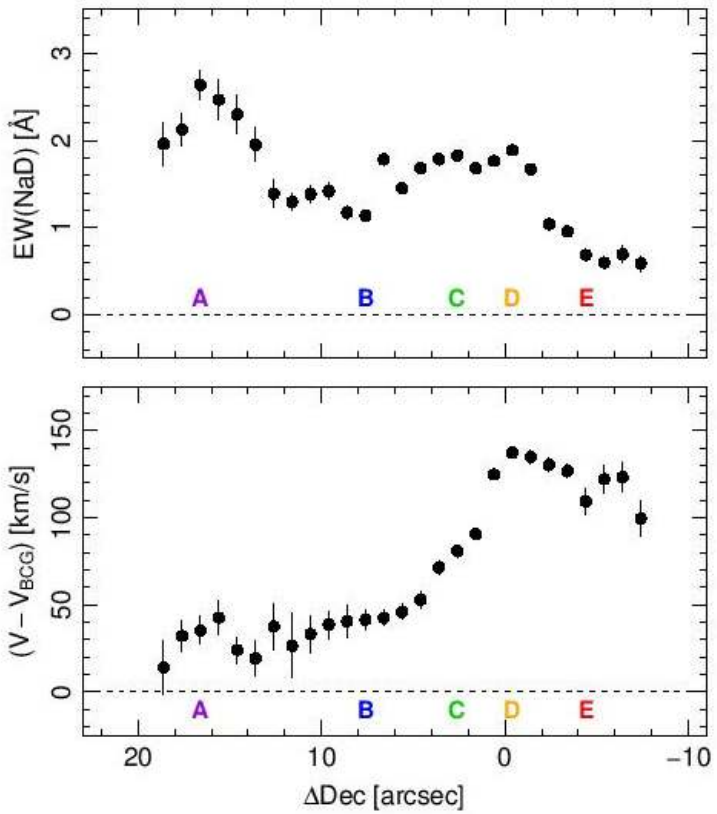

Figure 3. Profiles of equivalent width and radial velocity (relative to the BCG), along the locus of strongest absorption. The measurements are derived from double-gaussian fits to the BCG-corrected spectra, extracted in 2 arcsec diameter apertures spaced

Есть слабый эмиссионный спектр, но нет звездного населения

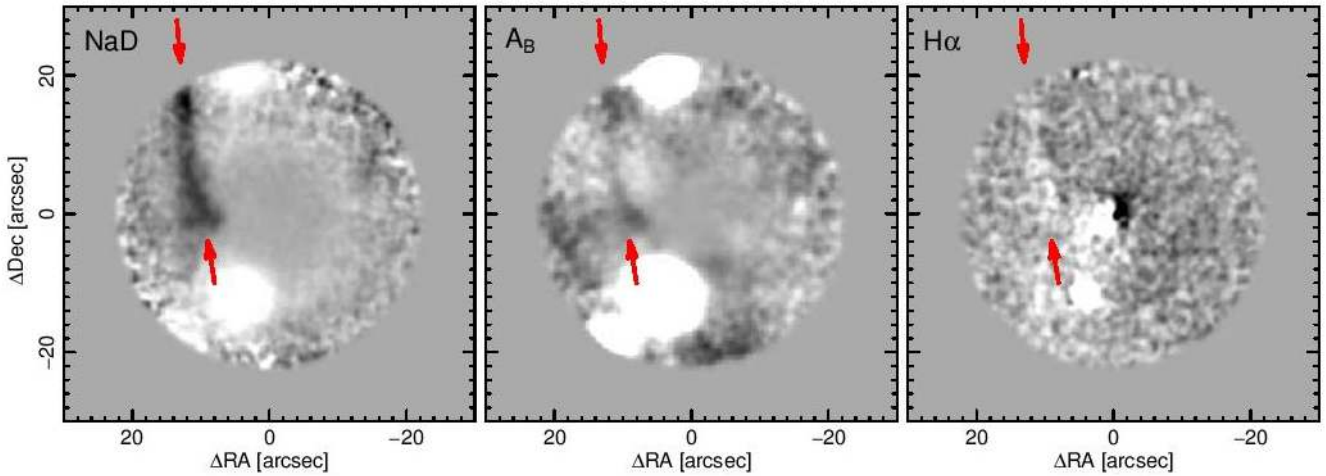

Figure 4. Faint hints at counterparts to the gas absorption in broadband extinction (shown as a ratio of WINGS B-band image to an ellipse-fit model), and Hα emission (from the MUSE data-cube). The Na D absorption image is reproduced at left, for comparison. Each image has been slightly smoothed to improve visibility.

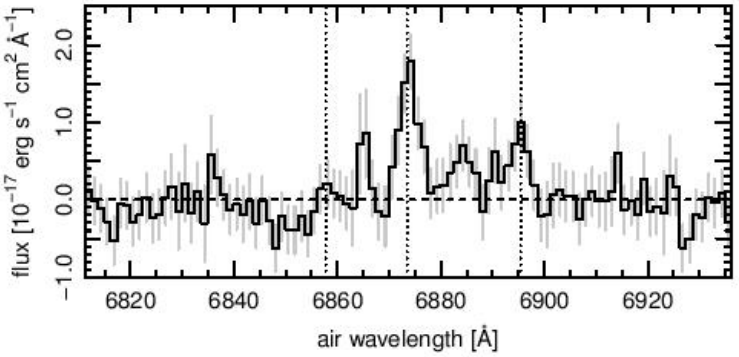

Figure 6. Net Hα-region spectrum extracted from pixels with EW(Na D) > 1 Å. Vertical lines show the wavelengths of the Hα and [N II] lines, at the redshift of the Na D absorption.

Astro-ph: 1706.08555

HI IN VIRGO'S "RED AND DEAD" DWARF ELLIPTICALS — A TIDAL TAIL AND CENTRAL STAR FORMATION

GREGORY HALLENBECK[1,2], REBECCA KOOPMANN[1], RICCARDO GIOVANELLI[3], MARTHA P. HAYNES[3], SHAN HUANG[4], LUKAS LEISMAN[3], EMMANOUIL PAPASTERGIS[5]

[1]Union College, Department of Physics & Astronomy, 807 Union Street, Schenectady NY 12308; hallenbg@union.edu, koopmanr@union.edu

[2]Washington & Jefferson College, Department of Computing and Information Studies, 60 S Lincoln Street, Washington PA, 15301.

[3]Cornell Center for Astrophysics and Planetary Science (CCAPS), Space Sciences Building, Cornell University, Ithaca, NY 14853; riccardo@astro.cornell.edu, haynes@astro.cornell.edu, leisman@astro.cornell.edu

[4]CCPP, New York University, 4 Washington Place, New York, NY 10003; shan.huang@nyu.edu

[5]Kapteyn Astronomical Institute, University of Groningen, Landleven 12, Groningen NL-9747AD, The Netherlands; papastergis@astro.rug.nl

ABSTRACT

We investigate a sample of 3 dwarf elliptical galaxies in the Virgo Cluster which have significant reservoirs of HI. We present deep optical imaging (from CFHT and KPNO), HI spectra (Arecibo) and resolved HI imaging (VLA) of this sample. These observations confirm their HI content and optical morphologies, and indicate that the gas is unlikely to be recently accreted. The sample has more in common with dwarf transitionals, although dwarf transitionals are generally lower in stellar mass and gas fraction. VCC 190 has an HI tidal tail from a recent encounter with the massive spiral galaxy NGC 4224. In VCC 611, blue star-forming features are observed which were unseen by shallower SDSS imaging.

Более ранний (2012) HI обзор

- Из 365 карликовых эллиптических галактик телескоп Аресибо зарегистрировал 7;
- Из них 2 позднее не подтвердились;
- Из остальных 2 позднее признаны проекциями;
- Осталось 3, которые решили рассмотреть пристальнее в этой работе

Красная последовательность и зеленая долина; HI – как у Irr-карликов

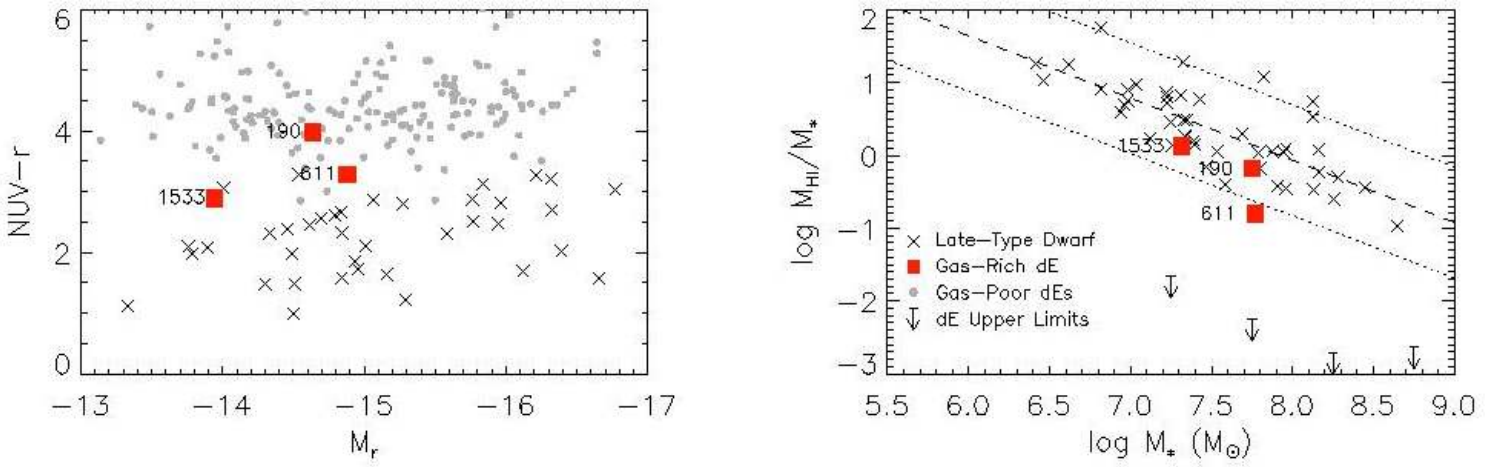

Figure 2. The 3 dwarf galaxies in our sample are red like typical dwarf ellipticals yet similar in gas richness to star-forming dwarf irregulars in the Virgo Cluster. (left) Ultraviolet and optical color-magnitude diagram of the dwarf galaxies in the Virgo Cluster. Crosses are late-type dwarfs with gas, gray circles are dwarf ellipticals without gas. Our sample of gas-bearing dwarf ellipticals are labeled with red squares. (right) Gas fraction as a function of stellar mass for late type dwarfs and our sample. Lines indicate the best fit and 2σ scatter for the late type dwarfs, and arrows are the 3σ upper limit for non-detected dwarf ellipticals based on stacking. All measurements are from Huang et al. (2012b) with updates in H12.

Стандартная dE-морфология

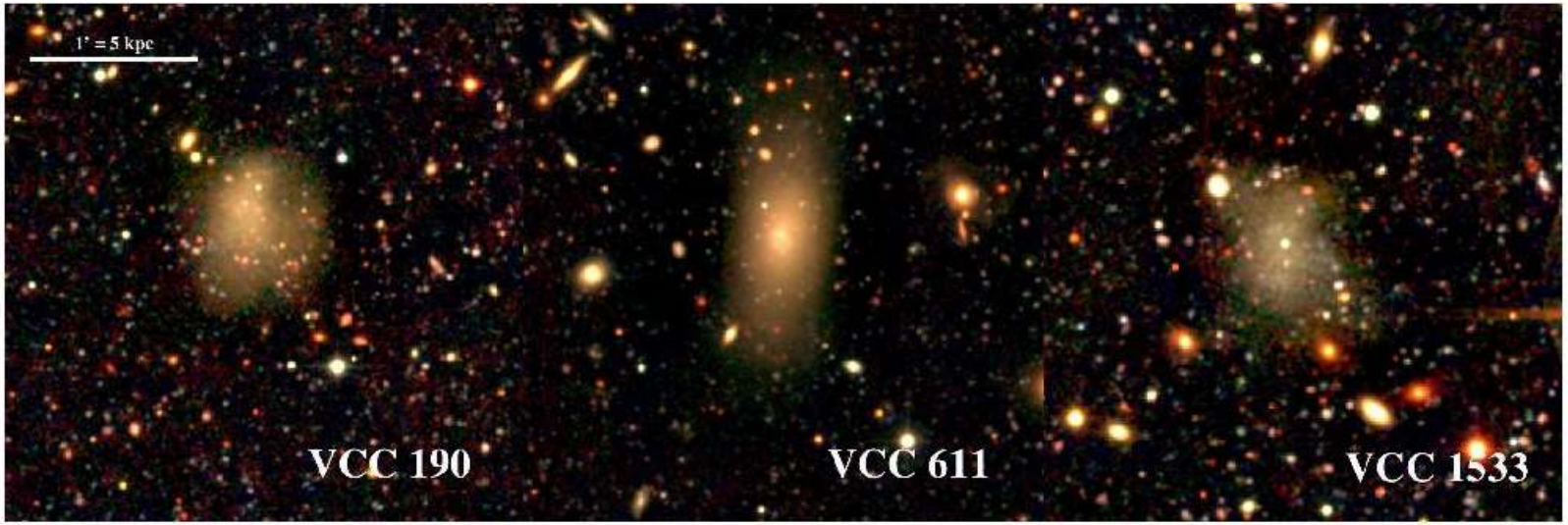

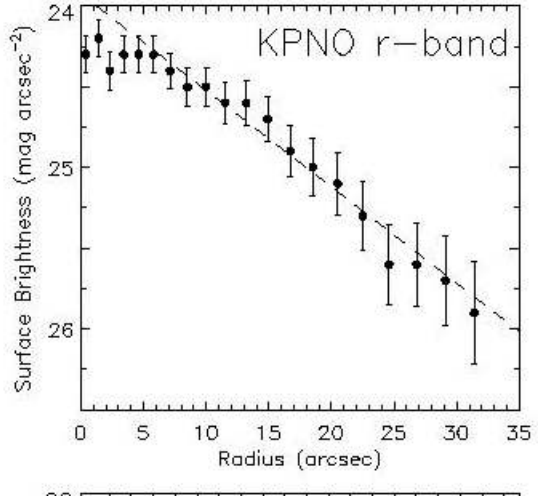

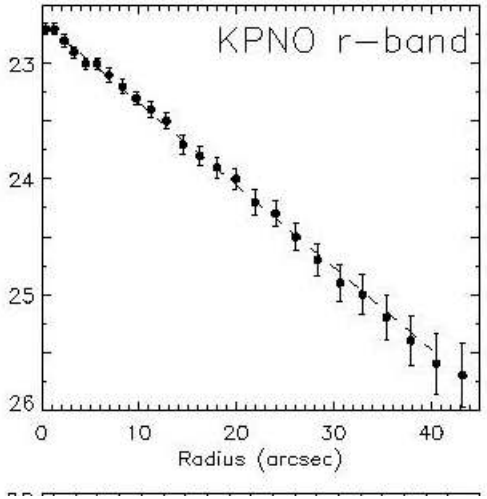

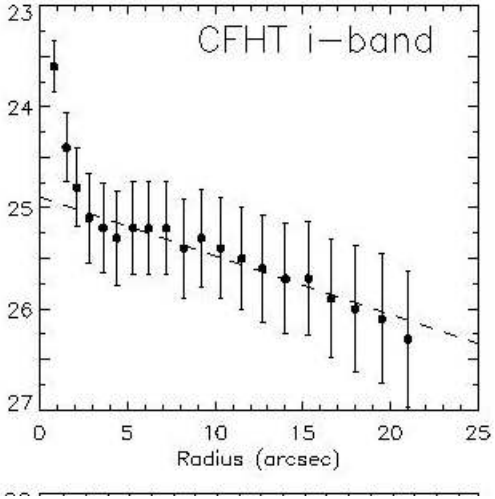

Интегральный профиль HI: нет вращения

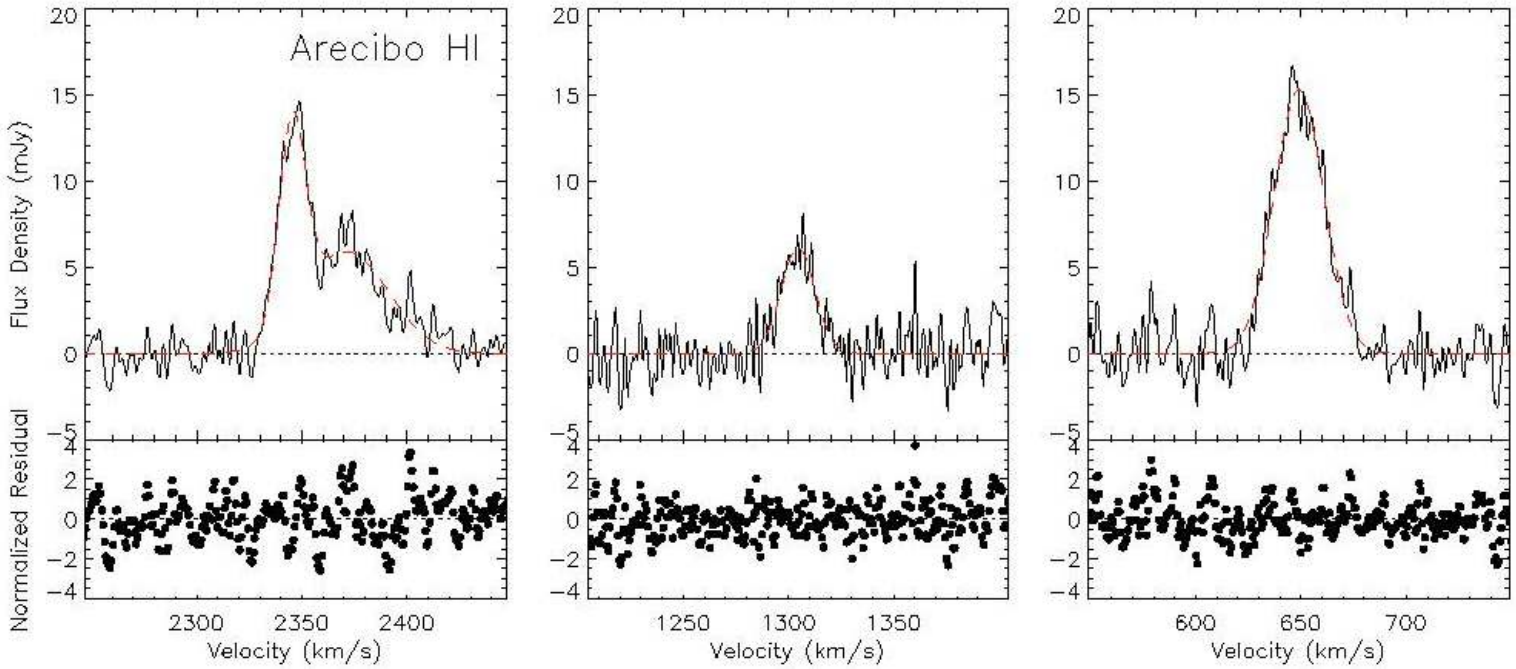

Table 2. Sample HI Properties

Galaxy	S_{HI} Jy km s^{-1} (1)	log M_{HI} log $M_\odot$ (2)	V_{sys} km s^{-1} (3)	W_{50} km s^{-1} (4)
VCC 190 A	0.18 ± 0.01	7.1	2345.4 ± 0.2	14.9 ± 0.6
VCC 190 B	0.29 ± 0.02	7.3	2371 ± 2	46 ± 2
VCC 611	0.12 ± 0.01	6.9	1304.5 ± 0.6	19 ± 1
VCC 1533	0.45 ± 0.01	7.5	648 ± 1	27.7 ± 0.6

VCC 190

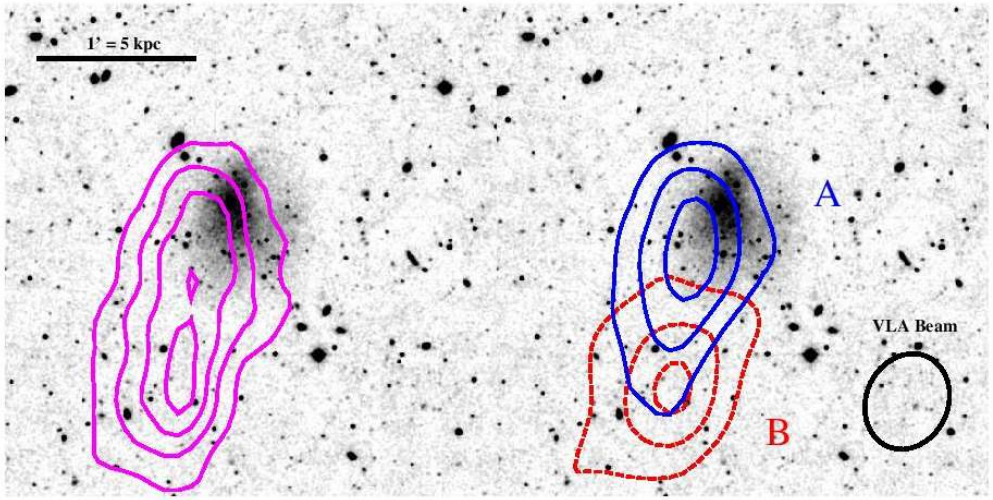

Figure 5. VLA HI intensity maps of VCC 190 overlaid on a KPNO *r*-band image. There are two separate reservoirs of gas in VCC 190. undisturbed component corresponding roughly to the optical center of the galaxy, and a wide (W_{50} = 50 km s^{-1}) component corresponding to tail. Contours begin at 3σ (0.03 Jy km s^{-1} beam^{-1} = 0.2 $M_{\odot}$ pc^{-2}) and increase by 3σ at each additional contour. (left) Intensity map includ gas at all velocities (right) Because the galaxy has two distince peaks, we produce two overlaid maps, one corresponding to the blueshi peak (v < 2343 km s^{-1}; blue solid contours) and the other for the redshifted velocity peak (v > 2343 km s^{-1}; red dashed contours). The lo velocity peak corresponds to gas coincident with the optical disk of the galaxy (VCC 190 A) while the higher velocity peak corresponds t HI tail (VCC 190 B).

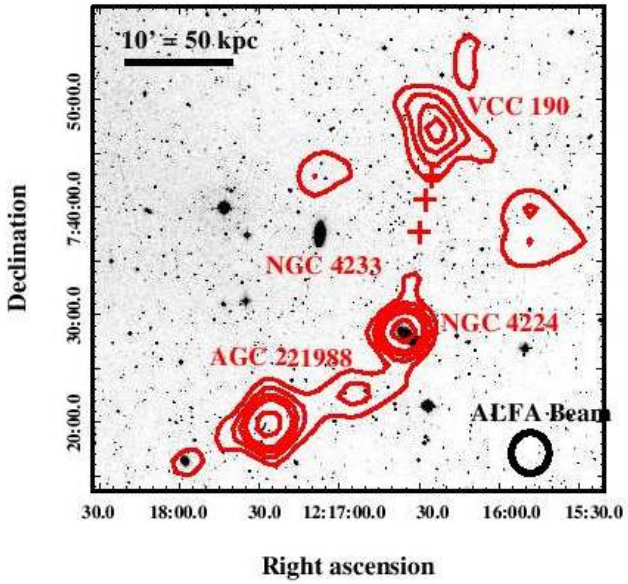

Figure 6. The environment of VCC 190. The tidal tail of VCC 190 points towards NGC 4224, suggesting a tidal encounter between the two. NGC 4224 is itself interacting with AGC 221988. Background is a DSS-2 composite optical image, while the overlaid contours are an HI column density map; contour levels are identical to Figure 1. All galaxies with redshifts consistent with the Virgo Cluster are labeled. The red crosses are the locations of additional Arecibo pointings used to detect a bridge between NGC 4224 and VCC 190; no gas was detected at any of the three pointings.

VCC 611

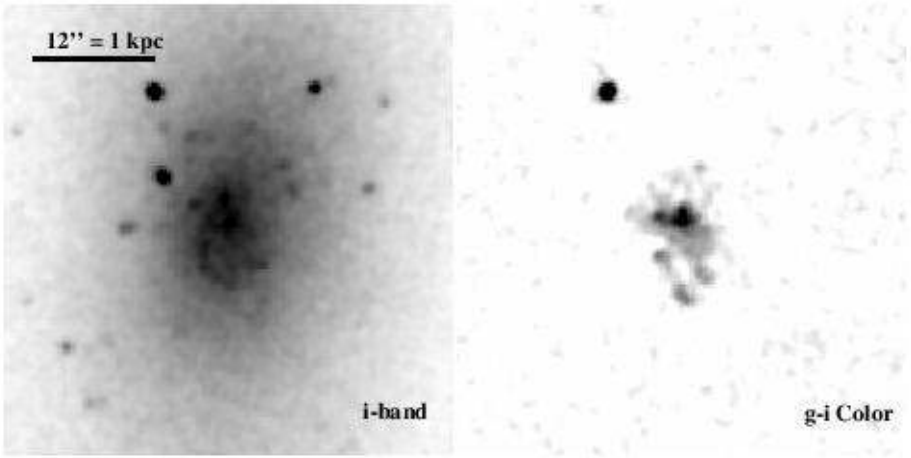

Figure 4. Deep CFHT images reveal that VCC 611 has strong star formation concentrated at the galaxy's center. (left) CFHT *i*-band image of the central 4 kpc of VCC 611. (right) $g-i$ color of the same field. The *i*-band image shows a mostly smooth old stellar population, while the $g-i$ color shows that star formation is occurring in the galaxy's center, in several star-forming knots.

Astro-ph: 1706.09461

Constraining cosmology with the velocity function of low-mass galaxies

Aurel Schneider[1] and Sebastian Trujillo-Gomez[2]
[1] *Institute for Astronomy, Department of Physics, ETH Zurich, Wolfgang-Pauli-Strasse 27, 8093, Zurich, Switzerland*
[2] *Institute for Computational Science, University of Zurich, Winterthurerstrasse 190, 8057 Zurich, Switzerland*
Email: aurel.schneider@phys.ethz.ch

30 June 2017

ABSTRACT
The number density of field galaxies per rotation velocity, referred to as the velocity function, is an intriguing statistical measure probing the smallest scales of structure formation. In this paper we point out that the velocity function is sensitive to small shifts in key cosmological parameters such as the amplitude of primordial perturbations (σ_8) or the total matter density (Ω_m). Using current data and applying conservative assumptions about baryonic effects, we show that the observed velocity function of the Local Volume favours cosmologies in tension with the measurements from `Planck` but in agreement with the latest findings from weak lensing surveys. While the current systematics regarding the relation between observed and true rotation velocities are potentially important, upcoming data from HI surveys as well as new insights from hydrodynamical simulations will dramatically improve the situation in the near future.

Модельные калибровки – ни при каком насилии над барионами не сходится с наблюдениями!

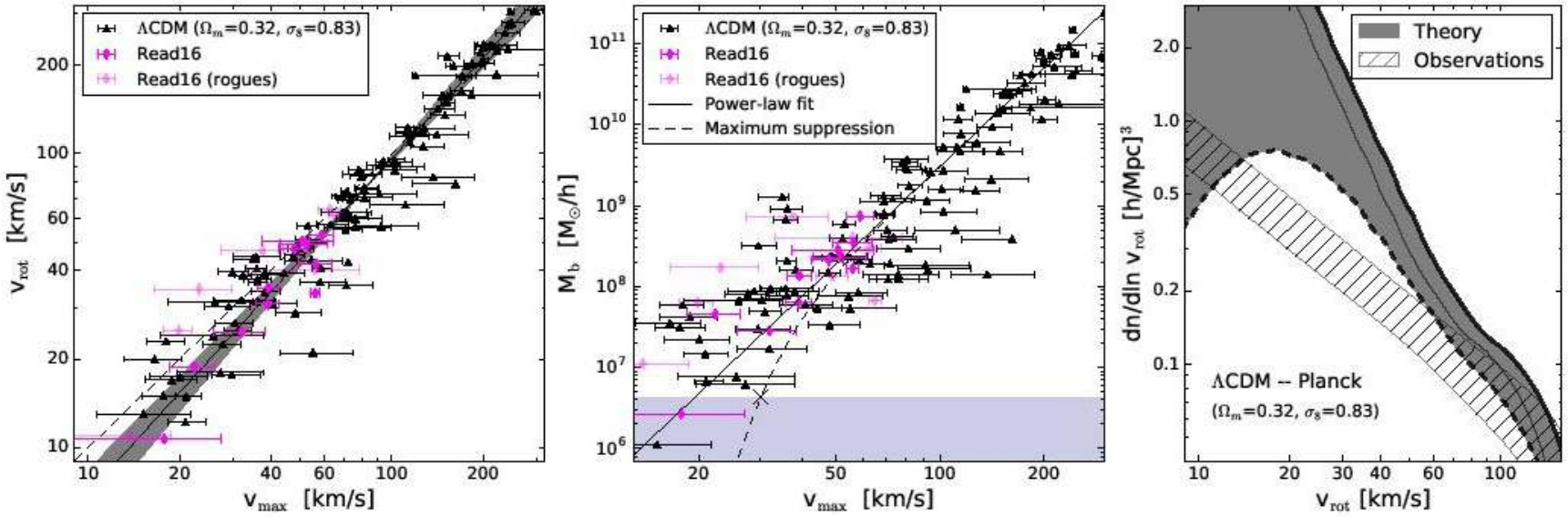

Figure 1. *Left:* relation between rotation velocity ($v_{\rm rot}$) and maximum circular velocity ($v_{\rm max}$) of selected galaxies with spatially resolved kinematics (black data points). The best-fit power-law including the 3-σ uncertainty of the fit is shown as solid line with grey-shaded band. For comparison, we add the results from Read16 (Read et al. 2016a) based on selected dwarf irregulars with high-quality rotation-curves (magenta symbols; the galaxies denoted *rogues* potentially suffer from systematics, see Read16). *Middle:* relation between baryonic mass ($M_{\rm b}$) and maximum circular velocity ($v_{\rm max}$) of the same galaxy sample. The solid line illustrates a simple power-law fit to the data, while the dashed line corresponds to a model featuring the maximum allowed suppression of baryonic mass due to photo-evaporation or supernova feedback (see text for more details). The data points from Read16 are again shown for comparison. *Right:* predicted number of observable galaxies per rotation velocity including uncertainties due to baryonic effects (grey area) compared to the observed velocity function of the Local Volume (hatched area, Klypin et al. 2015). The rotation velocity ($v_{\rm rot}$) is defined via the HI line-width (w_{50}) and the galaxy inclination (i), i.e., $v_{\rm rot} \equiv w_{50}/(2 \sin i)$. All three panels assume a ΛCDM universe with cosmological parameters from `Planck`.

… если только не предпочесть ранний WMAP Planck'у

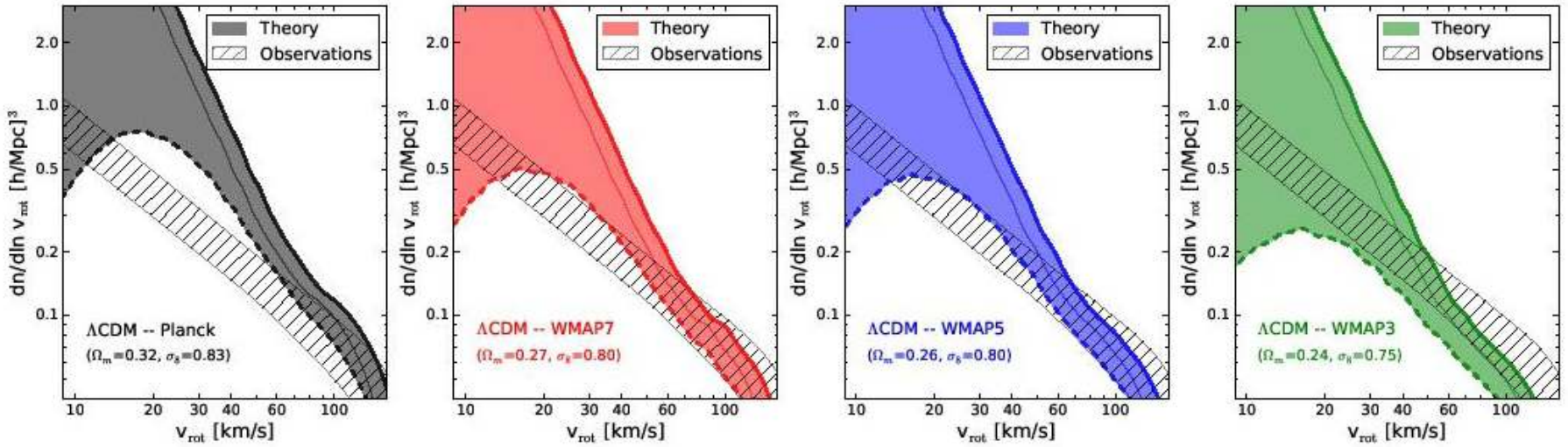

Figure 2. Velocity function for four different cosmologies based on `Planck` (black), `WMAP7` (red), `WMAP5` (blue), and `WMAP3` (green). The hatched areas correspond to the observed velocity function of the Local Volume including sample variance (Klypin et al. 2015). The colour-shaded areas show the theoretical predictions using our model to account for the effects of baryons. The solid and dashed lines enclosing the coloured areas represent the minimum and maximum baryonic modifications allowed by current data (see Sec. 2 for details). The rotation velocity ($v_{\rm rot}$) is defined via the HI line-width (w_{50}) and the galaxy inclination (i), i.e., $v_{\rm rot} \equiv w_{50}/(2\sin i)$.

Но, вообще говоря, результатам Планка еще много что противоречит

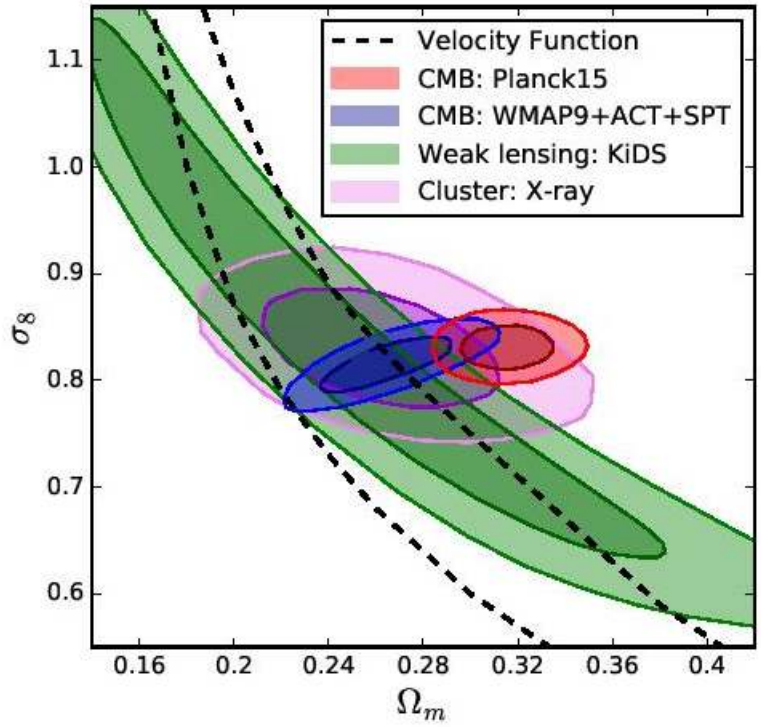

Figure 4. Combined constraints on Ω_m and σ_8 from the velocity function of galaxies in the Local Volume (dashed black line) with all other cosmological parameters kept at the fiducial values (see text). The contours from the CMB measurements `Planck` (red) and `WMAP9+ACT+SPT` (blue) as well as the weak lensing survey `KiDS` (green) and the cluster count observations of Mantz et al. (2015, magenta) are shown for comparison (bright and dark colours indicate 68% and 95% confidence levels)